

Crystallographic Orientation-Aligned ZnO Nanorods Grown by a Tin Catalyst

P. X. Gao, Y. Ding, and Z. L. Wang*

School of Materials Science and Engineering, Georgia Institute of Technology, Atlanta, Georgia 30332-0245

Received July 21, 2003; Revised Manuscript Received July 30, 2003

ABSTRACT

Well-aligned ZnO nanorods with identical crystallographic orientation have been synthesized using a vapor transport deposition process. Orientation-ordered nanorods grow normal to the *c* planes of the as-deposited micrometer-sized ZnO rods on a polycrystalline Al₂O₃ substrate, and each nanorod is along [0001] and enclosed by {2 $\bar{1}$ 10} facet surfaces. The nanorods remain in an identical crystal orientation with a homoepitaxial orientation relationship with the microrod. During the synthesis, reduced Sn from SnO₂ powder added to the source materials functions as a catalyst, guiding the orientation-aligned growth of ZnO nanorods. By controlling the growth time at high temperature, uniform lengths of aligned nanorods have been received. This work demonstrates that metallic Sn could be a good candidate for catalyzing the growth of 1D nanostructures.

Zinc oxide, a wide band gap (3.37 eV) semiconducting, piezoelectric, and photoconducting material, has a wide range of applications in solar cells,¹ sensors,^{2–4} optoelectronic devices, and surface acoustic waveguides.⁵ Recently, 1D nanostructures of ZnO, including nanowires,⁶ nanobelts,⁷ and nanotubes,⁸ have been attracting vast interest in the field of nanotechnology. Hierarchy and aligned ZnO nanostructures are finding potential applications in lasers,⁶ sensors,^{9,10} light-emitting diodes,¹¹ nanoresonators and cantilevers,^{12,13} and field-emission devices.^{14–16}

In syntheses of aligned 1D ZnO nanostructures, catalysts such as Au,^{6,17} Co,¹⁵ and NiO¹⁸ have been introduced into the synthesis process to guide the oriented growth of ZnO nanowires, and aligned growth without catalysis has also been achieved using low-temperature CVD (chemical vapor deposition)¹⁹ and ultrahigh vacuum deposition techniques such as MOCVD (metal–organic chemical vapor deposition)^{11,14} and MOVPE (metal–organic vapor-phase epitaxy).²⁰ In this letter, we report a novel method of synthesizing orientation-aligned ZnO nanorods and nanobelts using metallic Sn as a catalyst. The ZnO nanorods have an identical crystallographic orientation, and their lengths have been controlled via the deposition time.

A chemical vapor transport process^{6,17,21–23} was used for the syntheses of aligned ZnO nanorods and nanobelts. The experimental apparatus includes a horizontal tube furnace, a rotary pump system, and a gas supply system. A mixture of commercial ZnO, SnO₂, and graphite powders in a certain ratio (2:1:1 Zn/Sn/C) was placed in an alumina boat as the source material and positioned at the center of the alumina

tube. To investigate the duration time dependence on the growth of desired nanostructures, we conducted the deposition process at 1150 °C for 5, 15, 30, and 60 min under a constant pressure of 200 mbar and an Ar flow rate of 20 sccm (standard cubic centimeters per minute). The entire length of the tube furnace is 50 cm. The desired nanostructures were deposited onto an alumina substrate located 21 cm away from the center of the furnace in a temperature range of 550–600 °C. Morphological, chemical, and crystallographic characterizations of the as-prepared samples were carried out using scanning electron microscopy (SEM), transmission electron microscopy (TEM), and electron dispersive X-ray spectroscopy (EDS).

Figure 1 is a group of typical SEM images of the as-synthesized nanostructures on an alumina substrate after 5 min of deposition at 1150 °C, showing the initial growth characteristics of the desired nanostructure. Micrometer-sized ZnO rods (microrods) of irregular side surfaces but uniform flat (0001) surfaces of $\sim 3 \mu\text{m}$ are formed on the alumina substrate, which sometime show faceted side surfaces (Figure 1b). On each microrod, there are a number of nanorods oriented perpendicular to the (0001) plane, as were clearly depicted in Figure 1c and d, which are respectively the top and side views of the oriented ZnO nanorods. At the tip of each nanorod and nanobelt, there is a comparably sized Sn ball. The oriented nanorods dispersively distribute on the flat *c* plane of the microrods with uniform diameters ranging from 20–40 nm and an average height of about 40–80 nm.

Upon extending the growth time at 1150 °C to 15 min, it is shown in Figure 2 that the oriented ZnO nanorods get longer and some nanobelts grow out of the side surfaces of

* Corresponding author. E-mail: zhong.wang@mse.gatech.edu.

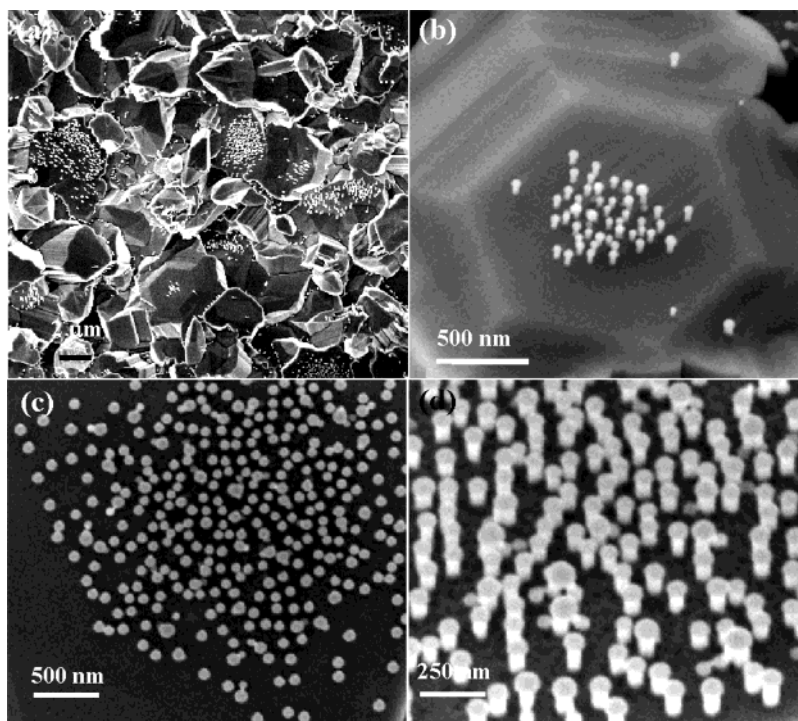


Figure 1. Initial growth of oriented nanorods using metallic Sn as the catalyst at 1150 °C with a growth time of 5 min. (a) Micrometer-scale ZnO short rods rooted on an Al₂O₃ substrate with aligned nanorods dispersively distributed on the top surfaces of the microrods. (b) Hexagonally faceted ZnO microrod with aligned ZnO nanorods on its top (0001) surface. (c, d) Top and side views, respectively, of the oriented ZnO nanorods on the top of a single-crystal microrod.

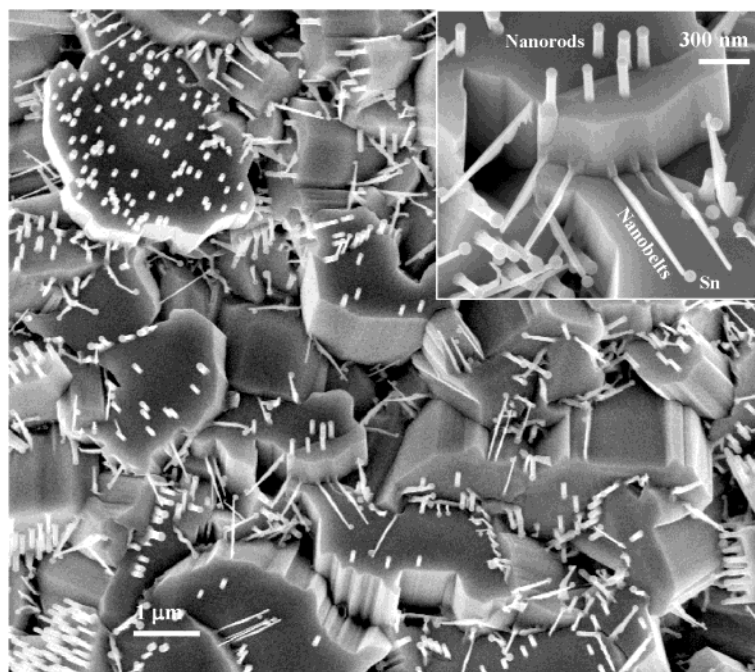


Figure 2. ZnO nanorods and nanobelts grown on the top and side surfaces of the ZnO microrods, respectively, after extending the growth time to 15 min. (Inset) Magnified SEM image.

the microrods. A higher-magnification picture clearly describes the perpendicular directional growth of the nanobelts (as indicated in the inset of Figure 2), where the nanorods have dimensions of 30–50 nm in diameter and 100–200 nm in length and nanobelts have dimensions of 10–30 nm in width and 300–500 nm in length.

The data suggest that the diameters of the nanorods are well confined by the size of the metallic Sn ball on the tip and that the growth time has a little influence on the diameter of the nanorods. Parts a and b of Figure 3 give a good description of the oriented growth of the nanorods on the *c* plane of the ZnO microrods. A closer examination of the

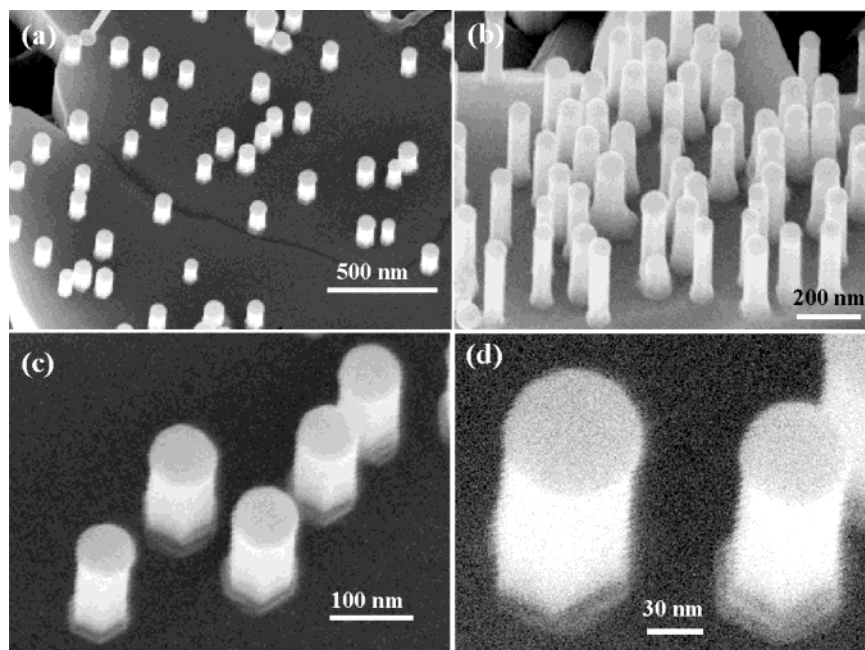


Figure 3. Perpendicular growth of nanorods on the c plane of ZnO microrods. (a, b) Dispersively oriented nanorods with inter-rod distances of ~ 400 and ~ 100 nm, respectively. (c, d) Epitaxial growth of the ZnO nanorods, forming arrays with an identical crystallographic orientation, as represented by the parallel side surfaces.

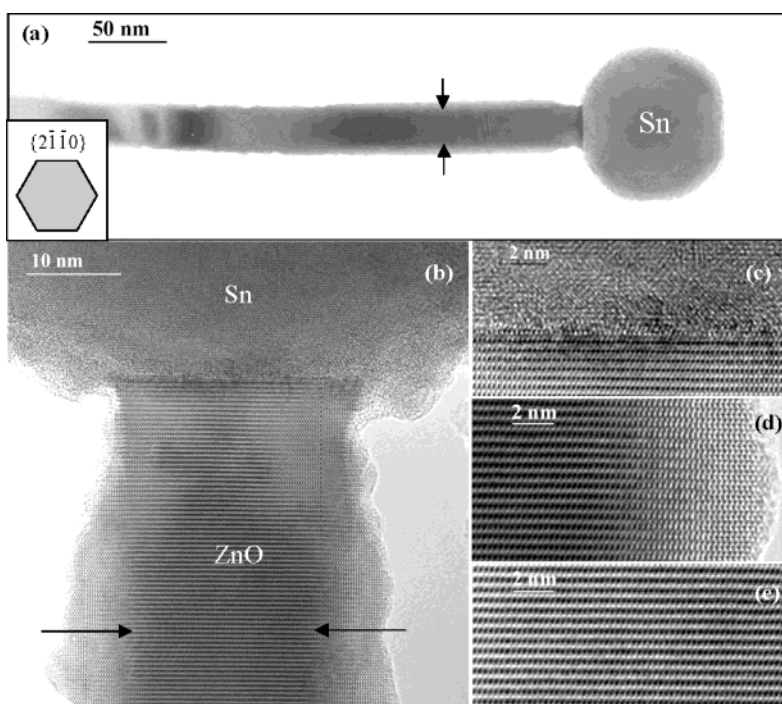


Figure 4. (a) Low-magnification TEM image of a ZnO nanorod with a model of its cross section in the inset. (b) High-resolution TEM image of the nanorod with the incident electron beam along $[21\bar{1}0]$. (c–e) Enlarged images from the Sn–ZnO interface, the edge of the nanorod, and the central region of the nanorod, respectively.

root of each nanorod in Figure 3c and d shows that each nanorod tends to grow along the same crystallographic orientation as the microrod with six parallel faceted surfaces of $\{2\bar{1}\bar{1}0\}$, which indicates an orientation alignment of the ZnO nanorods and a coherent epitaxial relationship with the base ZnO microrod.

Transmission electron microscopy imaging of a ZnO nanorod is presented in Figure 4. An Sn ball with a faceted

surface²⁴ is located at the growth front (Figure 4a). A high-resolution TEM image presented in Figure 4b shows that the ZnO nanorod grows along $[0001]$ and that its volume is free from dislocation. The interface between the Sn particle and the ZnO nanorod is atomically sharp and there may be a coherent relationship between the atomic lattices at the interface (Figure 4c), but the Sn is not well crystallized. From the image contrast across the nanorod presented in the low-

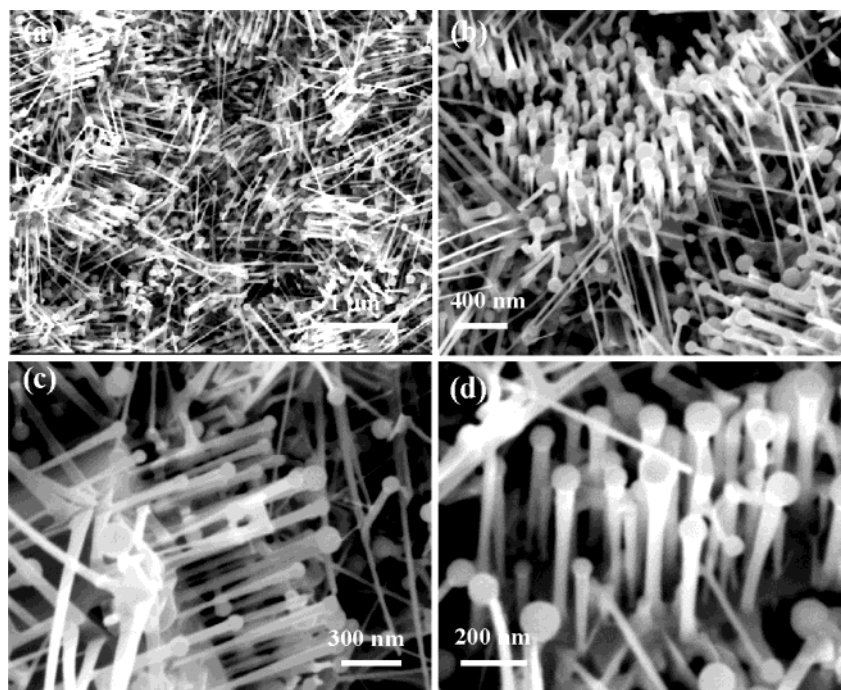


Figure 5. Typical morphology of the as-synthesized nanorods and nanobelts after 60 min of growth at 1150 °C. (a) Aligned ZnO nanorods and side-branched nanobelts on microrods. (b, c) Perpendicular orientation relationship between the oriented ZnO nanorods and the surrounding nanobelts on a single microrod as viewed from the top and the side, respectively. (d) Magnified view of the oriented nanorods rooted on a microrod.

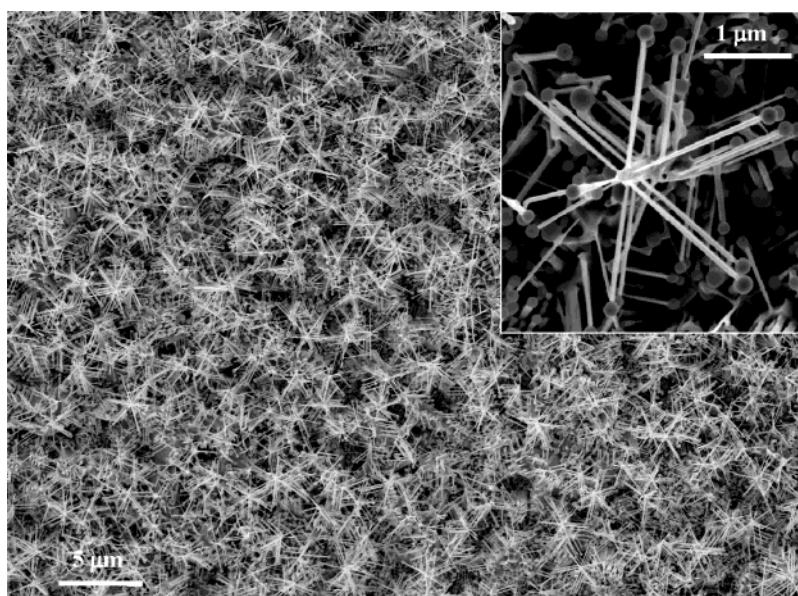


Figure 6. Top view of the well-aligned nanowire–nanobelt junction arrays on an alumina substrate. (Inset) Magnified micrograph of a single set of junction arrays with a 6-fold-symmetric structural feature.

magnification image (Figure 4a) and in the high-magnification TEM image in Figure 4b, a uniform contrast region at the middle of the nanorod (see the region indicated by arrows in Figure 4b and the enlarged image in Figure 4e) indicates its constant projected thickness, and the side edges are very thin (Figure 4d). On the basis of the image information, the six side surfaces of the nanorods are defined to be $\{2\bar{1}10\}$, and the electron beam direction is $[2\bar{1}\bar{1}0]$. A schematic model of the nanorod cross section is inserted into Figure 4a.

With increasing growth time, the oriented nanorods and nanobelts grew longer and longer. Figure 5 shows a typical morphology of the as-synthesized nanostructures upon 60 min at 1150 °C. Figure 5a shows the as-deposited nanostructures composed of the orientation-aligned ZnO nanorods and nanobelts out of the top and side surfaces of the microrods (Figure 5b and c). The ZnO nanorods grow out of the c plane with a uniform length of 0.5–1.0 μm , and the diameter remains around 30–60 nm. Compared to

those grown for a shorter time and separated by 100 nm–1 μm , these oriented nanorods grew densely with a separation of 50–150 nm, suggesting an increase in the number of nucleation sites during the growth. A slight increase in the diameter at the upper part of the nanorod is likely due to an increase in the size of the Sn catalyst particle during the growth. High-magnification images (Figure 5b and d) show that the microrods are rougher than those grown for 5 min. Along the perpendicular directions to the oriented nanorods, the number of side-branched nanobelts of a uniform length of 1 μm also dramatically increases. It is interesting that the metallic Sn head on the top of the nanorod is about one-third larger in diameter than the nanorod diameter and that the size of the Sn head on a nanobelt is about 2 to 3 times larger than the width of the nanobelt.

To study the effect of graphite as a vapor-generation agent for the growth of the desired nanostructures, an experimental session was conducted by adjusting the molar ratio of corresponding Zn/Sn/C from 2:1:1 to 2:1:2 while keeping the other parameters the same as for the experiments presented above and limiting the growth time to 1 h. Surprisingly, well-aligned nanowire–nanobelt junction arrays²¹ formed perpendicularly oriented on the alumina substrate. Figure 6 is a top view of the as-grown junction arrays over a large area, where the 6-fold-symmetric feature of each junction array is clearly seen. The inset is a typical magnified micrograph of a single junction array. Similar to the structure reported previously,²¹ the junction array consists of a central nanowire 100–200 nm in diameter and is surrounded by 6-fold-symmetric nanobelts 50–100 nm in width that grow along the six crystallographic equivalent directions of $\langle 01\bar{1}0 \rangle$.

Graphite is introduced into the raw material to increase the creation rate of Zn and Sn vapors. Carbon can reduce ZnO and SnO₂ in Zn and Sn vapors at relatively low temperature. It is expected that doubling the content of graphite in the raw material will increase the concentration of Sn liquid droplets, giving rise to many more nucleation sites²⁵ and leading to the growth of high-density nanorods and nanobelts. According to previous studies on junction arrays,²¹ it is known that the side-branched nanobelts would like to grow along six crystallographically equivalent orientations $\langle 01\bar{1}0 \rangle$, giving 6-fold-symmetric nanowire–nanobelt junction arrays presented in Figure 6.

To optimize the desired morphology of the oriented ZnO nanorods, we tested some more parameters. Figure 7 shows a typical morphology of the as-prepared nanorods and nanobelts after 30 min of growth at 1100 °C, where we used only two-thirds the amount of SnO₂ used in the other experiments and kept the pressure and argon flow rate the same. In Figure 7a, it is clearly shown that, in addition to the oriented ZnO nanorods, there are also some ZnO belt networks normal to and between the oriented nanorods, as indicated by arrows. These networks are parallel to the nanobelts directly growing from the side surfaces of the microrod base because of the homoepitaxial orientation relationship.²⁶ Figure 7b is a magnified view of the vertical crystallographic orientation-aligned ZnO nanorods on a ZnO

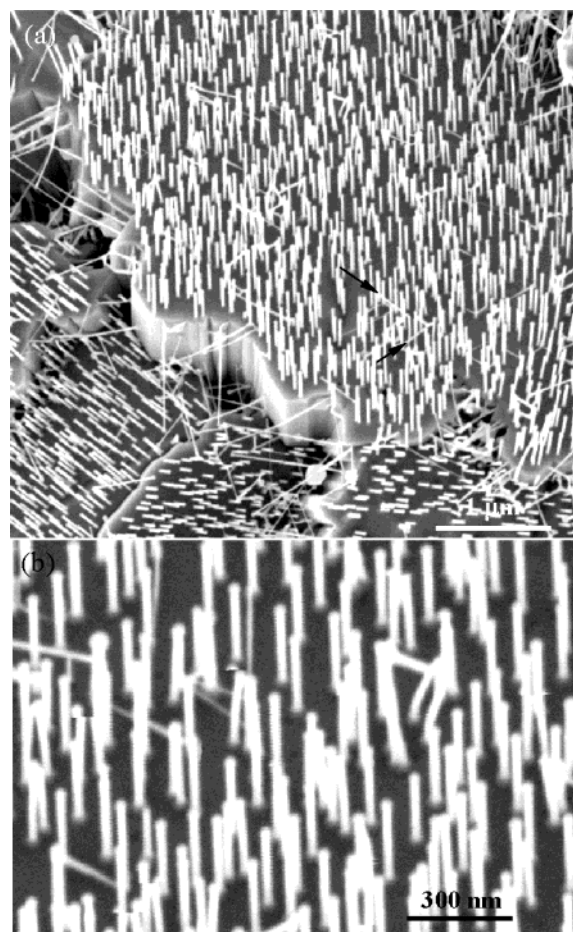


Figure 7. Typical morphology of the as-synthesized nanorods and nanobelts after 30 min of growth at 1100 °C. (a) Well-aligned nanorods on a larger surface area. Nanobelts grown out of the nanorods in a perpendicular direction are also identified, as indicated by arrows. The alignment in the nanobelt directions indicates the crystallographic-orientation ordering among the nanorods. (b) Magnified view of the crystallographically aligned ZnO nanorod arrays.

microrod, displaying a uniform diameter of ~ 25 nm and a height of ~ 250 nm.

There are two processes for the growth of ZnO nanorods. One is the oxidation of the reduced and vaporized Zn following the vapor–liquid–solid (VLS) growth process,^{6,21,27} and the other is the direct deposition of the ZnO vapor (the so-called vapor–solid (VS) process)⁷. On the basis of our experimental data presented here and published previously,^{28,29} reductions of ZnO and SnO₂ in Zn and Sn vapors, respectively, are possible in the high-temperature zone. The carrier gas transfers the reduced and vaporized Zn and Sn to the lower-temperature region. The oxidation of Zn vapor and its subsequent deposition onto the substrate form single-crystal ZnO microrods with flat (0001) surfaces. Simultaneously, Sn vapor would be transformed to liquid droplets falling down onto the surface of the ZnO microrods. Then, on these flat planes, dispersed metallic Sn droplets function as catalysts to guide the oriented growth of ZnO, which in fact is a homoepitaxial process with the bulk ZnO microrods.²⁶ The oriented nanorods remain in an identical orientation with the microrods, resulting in the crystal-

lographic orientation-aligned growth of the nanorods on the (0001) surface. However, the liquid tin droplets in contact with the side surface of the ZnO microrods guide the growth of ZnO nanobelts along $\langle 01\bar{1}0 \rangle$ perpendicular to the ZnO nanorods. A continuous deposition of Sn vapor at the growth front results in a continuous increase in the size of the Sn particle, leading to a continuous increase in the size of the nanorods/nanobelts as growth proceeds.

Our data suggest that the VLS process is dominant and the VS process is supplementary. As presented in Figure 1d, the microrods as the growth platforms are quite rough at the very beginning between the oriented nanorods and even form deep notches as if they were etched off at longer growth times. Then it is expected that, as the growth time increases, the source materials are consumed, the supply of vapors is short, and the vapor pressure may fall below the supersaturation threshold required for VLS growth. The growth can be continued only by vaporizing the microrods below the nanorods, resulting in the deep notches on microrod surfaces.

In summary, by using a simple vapor-transport deposition method, well-aligned ZnO nanorods with six identical facets of $\{2\bar{1}\bar{1}0\}$ and orientation ordering have been successfully synthesized. Reduced Sn from SnO₂ acts as a catalyst that guides the aligned growth of ZnO nanorods. By controlling the growth time at high temperature, nanorods of uniform lengths have been produced. By increasing the content of graphite as the vapor-generating agent, well-aligned nanowire–nanobelt junction arrays have also been received. This study demonstrates that Sn can be an effective catalyst that can be used to grow crystallographic orientation-aligned nanorods.

Acknowledgment. We are grateful for financial support from the NASA URETI program.

References

- (1) Keis, K.; Vayssieres, L.; Lindquist, S.; Hagfeldt, A. *Nanostruct. Mater.* **1999**, *12*, 487.
- (2) Minne, S. C.; Manalis, S. R.; Quate, C. F. *Appl. Phys. Lett.* **1995**, *67*, 3918.
- (3) Shibata, T.; Unno, K.; Makino, E.; Ito, Y.; Shimada, S. *Sens. Actuators, A* **2002**, *102*, 106.
- (4) Lin, H. M.; Tzeng, S. J.; Hsiau, P. J.; Tsai, W. L. *Nanostruct. Mater.* **1999**, *10*, 465.
- (5) Gorla, C. R.; Emanetoglu, N. W.; Liang, S.; Mayo, W. E.; Lu, Y.; Wraback, M.; Shen, H. *J. Appl. Phys.* **1999**, *85*, 2595.
- (6) Huang, M. H.; Mao, S.; Feick, H.; Yan, H. Q.; Wu, Y. Y.; Kind, H.; Weber, E.; Russo R.; Yang, P. D. *Science* **2001**, *292*, 1897.
- (7) Pan, Z. W.; Dai Z. R.; Wang, Z. L. *Science* **2001**, *291*, 1947.
- (8) Wu, J. J.; Liu, S. C.; Wu, C. T.; Chen, K. H.; Chen, L. C. *Appl. Phys. Lett.* **2002**, *81*, 1312.
- (9) Arnold, M. S.; Avouris, P.; Pan, Z. W.; Wang, Z. L. *J. Phys. Chem. B* **2003**, *107*, 659.
- (10) Comini, E.; Faglia, G.; Sberveglieri, G.; Pan, Z. W.; Wang, Z. L. *Appl. Phys. Lett.* **2003**, *81*, 1869.
- (11) Park, W. I.; Yi, G. C.; Kim, J. W.; Park, S. M. *Appl. Phys. Lett.* **2003**, *82*, 4358.
- (12) Bai, X. D.; Gao, P. X.; Wang, Z. L.; Wang, E. G. *Appl. Phys. Lett.* **2003**, *82*, 4806.
- (13) Hughes, W.; Wang, Z. L. *Appl. Phys. Lett.* **2003**, *82*, 2886.
- (14) Park, W. I.; Yi, G.; Kim, M.; Pennycook, S. L. *Adv. Mater.* **2002**, *14*, 1841.
- (15) Lee, C. J.; Lee, T. J.; Lyu, S. C.; Zhang, Y.; Ruh, H.; Lee, H. J. *Appl. Phys. Lett.* **2002**, *19*, 3648.
- (16) Bai, X. D.; Wang, E. G.; Gao, P. X.; Wang, Z. L. *Nano Lett.*, in press, 2003.
- (17) Ng, H. T.; Li, J.; Smith, M. K.; Nguyen, P.; Cassell, A.; Han, J.; Meyyanpan, M. *Science* **2003**, *300*, 1249.
- (18) Lyu, S. C.; Zhang, Y.; Ruh, H.; Lee, H. J.; Shim, H. W.; Suh, E. K.; Lee, C. J. *Chem. Phys. Lett.* **2002**, *363*, 134.
- (19) Wu, J.-J.; Liu, S.-C. *Adv. Mater.* **2002**, *14*, 215.
- (20) Ogata, K.; Maejima, K.; Fujita, Sz.k; Fujita, Sg. *J. Cryst. Growth* **2003**, *248*, 25.
- (21) Gao, P. X.; Wang, Z. L. *J. Phys. Chem. B* **2002**, *106*, 12653.
- (22) Lao, J. Y.; Wen, J. G.; Ren, Z. F. *Nano Lett.* **2002**, *2*, 1287.
- (23) Hassani, S.; Tromson-Carli, A.; Lusson, A.; Didier, G.; Triboulet, R. *Phys. Status Solidi B* **2002**, *229*, 835.
- (24) Zhu, Y. Q.; Hsu, W. K.; Zhou, W. Z.; Terrones, M.; Kroto, H. W.; Walton, D. R. M. *Chem. Phys. Lett.* **2001**, *347*, 337.
- (25) Abduev, A. K.; Akhmedov, A. K.; Baryshnikov, V. G.; Shakhshaev, Sh. O. *Tech. Phys. Lett.* **2000**, *4*, 37.
- (26) Ogata, K.; Kawanishi, T.; Maejima, K.; Fujita, Sz.; Fujita, Sg. *J. Cryst. Growth* **2002**, *237–239*, 553.
- (27) Wagner, R. S.; Ellis, W. C. *Appl. Phys. Lett.* **1964**, *4*, 89.
- (28) Dai, Z. R.; Pan, Z. W.; Wang, Z. L. *J. Am. Chem. Soc.* **2002**, *124*, 8673.
- (29) Gao, P. X.; Wang, Z. L. *J. Am. Chem. Soc.*, in press, 2003.

NL034548Q